# KRN951, a Highly Potent Inhibitor of Vascular Endothelial Growth Factor Receptor Tyrosine Kinases, Has Antitumor Activities and Affects Functional Vascular Properties

Kazuhide Nakamura,[1] Eri Taguchi,[1] Toru Miura,[1] Atsushi Yamamoto,[1] Kazumi Takahashi,[1] Francis Bichat,[3] Nicolas Guilbaud,[3] Kazumasa Hasegawa,[2] Kazuo Kubo,[2] Yasunari Fujiwara,[2] Rika Suzuki,[2] Kinya Kubo,[2] Masabumi Shibuya,[4] and Toshiyuki Isoe[2]

[1]Pharmaceutical Development Laboratories and [2]Pharmaceutical Research Laboratories, Kirin Brewery, Co., Ltd., Takasaki, Gunma, Japan; [3]Oncodesign S.A., Dijon, France; and [4]Division of Genetics, Institute of Medical Science, University of Tokyo, Tokyo, Japan

## Abstract

**Vascular endothelial growth factor (VEGF) plays a key role in tumor angiogenesis by stimulating the proangiogenic signaling of endothelial cells via activation of VEGF receptor (VEGFR) tyrosine kinases. Therefore, VEGFRs are an attractive therapeutic target for cancer treatment. In the present study, we show that a quinoline-urea derivative, KRN951, is a novel tyrosine kinase inhibitor for VEGFRs with antitumor angiogenesis and antigrowth activities. KRN951 potently inhibited VEGF-induced VEGFR-2 phosphorylation in endothelial cells at *in vitro* subnanomolar $IC_{50}$ values ($IC_{50}$ = 0.16 nmol/L). It also inhibited ligand-induced phosphorylation of platelet-derived growth factor receptor-β (PDGFR-β) and c-Kit ($IC_{50}$ = 1.72 and 1.63 nmol/L, respectively). KRN951 blocked VEGF-dependent, but not VEGF-independent, activation of mitogen-activated protein kinases and proliferation of endothelial cells. In addition, it inhibited VEGF-mediated migration of human umbilical vein endothelial cells. Following p.o. administration to athymic rats, KRN951 decreased the microvessel density within tumor xenografts and attenuated VEGFR-2 phosphorylation levels in tumor endothelium. It also displayed antitumor activity against a wide variety of human tumor xenografts, including lung, breast, colon, ovarian, pancreas, and prostate cancer. Furthermore, dynamic contrast-enhanced magnetic resonance imaging (DCE-MRI) analysis revealed that a significant reduction in tumor vascular hyperpermeability was closely associated with the antitumor activity of KRN951. These findings suggest that KRN951 is a highly potent, p.o. active antiangiogenesis and antitumor agent and that DCE-MRI would be useful in detecting early responses to KRN951 in a clinical setting. KRN951 is currently in phase I clinical development for the treatment of patients with advanced cancer.** (Cancer Res 2006; 66(18): 9134-42)

## Introduction

Vascular endothelial growth factor (VEGF) is involved in tumor angiogenesis and plays an important role in tumor malignancy, such as sustaining tumor growth and in blood-borne metastasis. VEGF regulates both vascular growth and permeability, and it also functions as an antiapoptotic factor for newly formed vessels (1). VEGF expression is up-regulated by changes associated with cancer, such as hypoxia, proto-oncogene activation, loss of tumor suppressor gene expression, and growth factor stimuli in tumors (1, 2). Its overexpression has been reported to correlate with the degree of vascularity, poor prognosis, and aggressive disease in the majority of human solid tumors (3–6) and in some hematopoietic malignancies (7).

Two high-affinity cognate endothelial receptors for VEGF have been identified (8, 9): VEGF receptor-1 (VEGFR-1; also known as Flt-1) and VEGFR-2 [also known as kinase insert domain-containing receptor (KDR)/Flk-1]. Both are members of a large family of receptor tyrosine kinases, and are almost exclusively located in endothelial cells. Activation of VEGFR-1 and VEGFR-2 receptors occurs through VEGF binding, which triggers receptor dimerization, tyrosine kinase activation, and phosphorylation of tyrosine residues. Although the affinity of VEGF for VEGFR-1 is higher than for VEGFR-2, the major mitogenic, angiogenic, and permeability-enhancing effects of VEGF seem to be mediated through VEGFR-2.

Several experimental approaches aimed at blocking VEGF signaling have shown that VEGF and its receptors are not only essential molecules for tumor angiogenesis, but are also attractive targets for cancer therapy (10). These approaches included the use of VEGF-neutralizing monoclonal antibodies, antibodies against VEGF receptors, recombinant soluble receptors, a tetracycline-regulated VEGF expression system, a dominant-negative VEGF receptor mutant, and small-molecule inhibitors of VEGFR tyrosine kinases. Among these, antibodies and small molecules were further developed as practical agents for cancer treatment both in preclinical and clinical settings (11). In particular, bevacizumab, a recombinant humanized monoclonal antibody to VEGF, has been approved as a first-line therapy for metastatic colorectal cancer (12). In addition, several VEGFR tyrosine kinase inhibitors are currently under preclinical or clinical development (13–21). Recently, two small-molecule inhibitors with activities against VEGFR tyrosine kinase, BAY 43-9006 (17) and SU11248 (14), have been approved for the treatment of patients with advanced renal cell cancer.

In the present study, we describe a novel quinoline-urea derivative, which is a highly potent VEGFR tyrosine kinase inhibitor, and also highlight the potential of using dynamic contrast-enhanced magnetic resonance imaging (DCE-MRI) to assess treatment responses.

## Materials and Methods

**KRN951.** *N*-{2-Chloro-4-[(6,7-dimethoxy-4-quinolyl)oxy]phenyl}-*N*′-(5-methyl-3-isoxazolyl) urea hydrochloride monohydrate (KRN951; Fig. 1*A*)

**Note:** Supplementary data for this article are available at Cancer Research Online (http://cancerres.aacrjournals.org/).

**Requests for reprints:** Kazuhide Nakamura, Pharmaceutical Development Laboratories, Kirin Brewery, Co., Ltd., 3 Miyahara, Takasaki, Gunma 370-1295, Japan. Phone: 81-27-346-9423; Fax: 81-27-347-5280; E-mail: ka-nakamura@kirin.co.jp.



doi:10.1158/0008-5472.CAN-05-4290

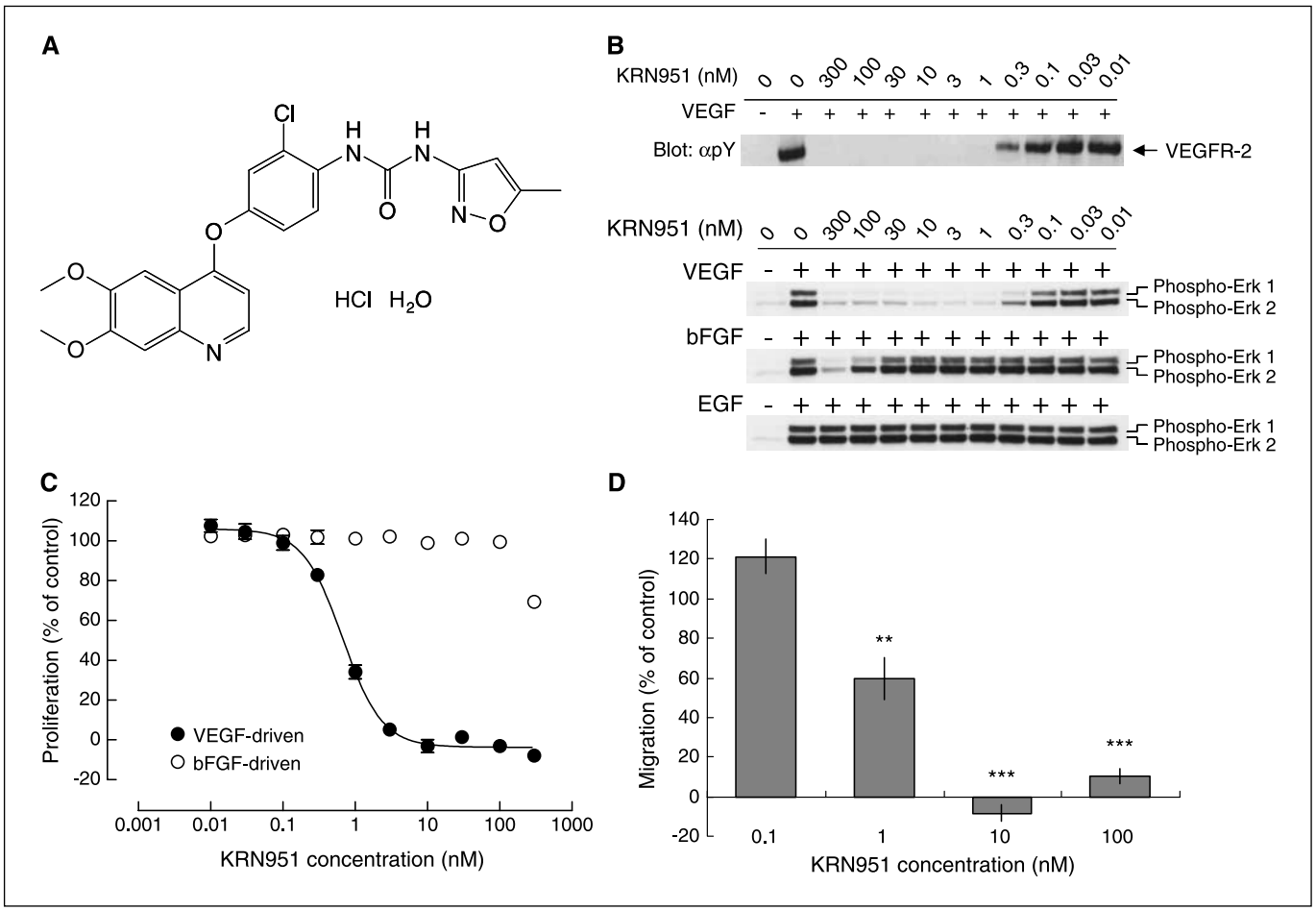


**Figure 1.** Inhibition of VEGF signaling in endothelial cells by KRN951. *A,* chemical structure of KRN951. *B,* serum-starved HUVECs were treated with KRN951 at the doses indicated and then stimulated with VEGF, bFGF, or EGF. VEGFR-2 was immunoprecipitated with an antireceptor antibody followed by immunoblotting with an antiphosphotyrosine monoclonal antibody (see Table 1 for the $IC_{50}$ of KRN951). MAPK phosphorylation was detected by immunoblotting with an anti–phosphorylated MAPK antibody. Similar results were obtained in four independent experiments. *C,* HUVEC proliferation was tested in a [$^3$H]thymidine incorporation assay ($n = 12$). Basal values for 100% and 0% proliferation were determined in the presence and absence of each ligand stimulus, respectively, in cultures containing 0.1% DMSO. *D,* HUVEC migration was tested using a 96-well microchamber plate ($n = 10$). Basal values for 100% and 0% migration were determined in the presence and absence of 10 ng/mL VEGF stimulus, respectively, in cultures containing 0.1% DMSO. *P* values were calculated with respect to the control (100% migration) using Dunnett's test. **, $P < 0.01$; ***, $P < 0.001$.

was synthesized in the Production Department, Research and Development Center, Kirin Brewery, Co., Ltd. (Tokyo, Japan). For *in vitro* studies, KRN951 was dissolved in DMSO and diluted in growth medium immediately before use. For *in vivo* studies, it was suspended in vehicle (0.5% methyl cellulose in distilled water) and the suspension was administered to animals within a day of preparation.

**Cell lines.** Human umbilical vein endothelial cells (HUVEC) and normal human dermal fibroblasts were obtained from Cambrex (Walkersville, MD). VEGFR-1–overexpressing NIH3T3 cells, designated NIH3T3-Flt-1, have been described previously (22). Colo205 (human colon carcinoma) and KU812-F (human chronic myelogenous leukemia) cells were obtained from the Cell Resource Center for Biomedical Research, Tohoku University (Sendai, Japan). The A431 (human epidermoid carcinoma) cell line was obtained from the Health Science Research Resources Bank (Osaka, Japan). A549 (human lung carcinoma) and EoL-1 (human eosinophilic leukemia) cells were obtained from the Institute of Physical and Chemical Research (Tsukuba, Japan). The CGL-9 (human glioma) cell line was obtained by mechanical dissociation of a s.c. SNB 19 (human glioma) tumor xenografted in athymic rats. All other cell lines were purchased from the American Type Culture Collection (Manassas, VA) unless otherwise specified.

**Kinase selectivity.** Cell-free kinase assays were done in quadruplicate with 1 μmol/L ATP to determine the $IC_{50}$ values of KRN951 against a variety of recombinant receptor and nonreceptor tyrosine kinases. Recombinant enzymes were obtained from ProQinase GmbH (Freiburg, Germany).

Cell-based assays were done to determine the ability of KRN951 to inhibit ligand-dependent phosphorylation of receptor tyrosine kinases as described previously (19). Briefly, the cells were starved overnight in appropriate basic medium containing 0.5% fetal bovine serum (FBS). Following the addition of KRN951 or 0.1% DMSO, the cells were incubated for 1 hour and then stimulated with the cognate ligand at 37°C. Receptor phosphorylation was induced for 5 minutes except for VEGFR-3 (10 minutes), c-Met (10 minutes), and c-Kit (15 minutes). All the ligands used in the assays were human recombinant proteins, except for VEGF-C, a rat recombinant protein. Following cell lysis, receptors were immunoprecipitated with appropriate antibodies and subjected to immunoblotting with phosphotyrosine. Quantification of the blots and calculation of $IC_{50}$ values were carried out as described previously (19).

**Mitogen-activated protein kinase activation.** This was evaluated as described previously (19). Briefly, HUVECs were starved for 16 hours in a basic medium (EBM-2, Cambrex) containing 0.5% FBS. Following incubation with KRN951 for 1 hour, HUVECs were stimulated with 50 ng/mL VEGF (PeproTech EC, Ltd., London, United Kingdom), 25 ng/mL basic fibroblast growth factor (bFGF; Upstate Biotechnology, Charlottesville, VA) or 20 ng/mL EGF (PeproTech EC.). Cell lysates were subjected to SDS-PAGE followed

by immunoblotting of phosphorylated MAPKs with phosphorylated p44/42 mitogen-activated protein kinase (MAPK) antibody (Cell Signaling Technology, Inc., Beverly, MA).

**Endothelial cell proliferation.** HUVECs were seeded in M-199 (Invitrogen, Carlsbad, CA) containing 5% FBS in collagen-coated 96-well plates (BD Biosciences, Bedford, MA) at a density of 4,000 cells/200 μL/well. After 24 hours, KRN951 was added followed by 20 ng/mL VEGF or 10 ng/mL bFGF, and the cells were cultured for 72 hours. [$^3$H]thymidine (1 μCi/mL) was added and the cells were cultured for a further 12 hours. Cells were then harvested and their radioactivity was measured with a Liquid Scintillation Counter (Wallac 1205 Beta Plate; Perkin-Elmer Life Sciences, Boston, MA).

**Chemotaxis assay.** HUVEC migration was assessed using 96-well microchamber plates (BD BioCoat Angiogenesis System, BD Biosciences). Cells were starved for 5 hours in EBM-2 containing 0.1% bovine serum albumin (BSA). Then, cells were harvested, resuspended in EBM-2 containing 0.1% BSA, and placed in the upper chamber. Cell migration was initiated by placing medium containing 10 ng/mL VEGF, 0.1% FBS, and 0.1% BSA to the bottom chamber. When indicated, KRN951 was added to both the upper and lower chambers. After 22 hours of incubation, cells were stained with 4 μg/mL calcein AM in HBSS. Fluorescence in the cells that had migrated through the pores of the fluorescence blocking membrane was directly measured through the bottom of the chambers in a fluorescence plate reader at excitation/emission wavelengths of 485/530 nm.

**Cytotoxicity assays.** These assays were done as described previously (19). Briefly, cells were seeded in 96-well plates and cultured in medium containing 10% FBS. KRN951 was added ~24 hours after the start of culture and the cells were then incubated for 72 hours. WST-1 reagent (Roche Applied Science, Indianapolis, IN) was used for the detection of cell viability.

**Measurement of phosphorylated VEGFR-2 levels and detection of tumor microvessels.** Athymic rats (F344/N Jcl-rnu) were obtained from CLEA Japan, Inc. (Tokyo, Japan). A549 tumor xenografts were established in rats by s.c. implantation of cells. Drug treatments were initiated when tumor volumes reached an average of 500 mm$^3$. Rats were randomized and then treated p.o. with KRN951 or vehicle, as described in the legends to the figures and table notes. To measure levels of VEGFR-2 phosphorylation in endothelial cells, tumor cryosections were processed for immunofluorescence staining with antiphosphorylated VEGFR-2 antibody (Spring Bioscience, Fremont, CA) and biotinylated secondary anti-rabbit IgG (Vector Laboratories, Burlingame, CA). Signals were amplified by the TSA fluorescence system (Perkin-Elmer, Wellesley, MA). Then, immunofluorescence staining of tumor microvessels was done with biotinylated anti-rat CD31 antibody as described previously (19).

**Tumor xenograft models.** Athymic rats (RH-rnu/rnu) were obtained from Harlan (Gannat, France). Twenty-four hours after whole body irradiation with a γ-source (7 Gy, Co$^{60}$), cancer cells were s.c. inoculated into the right flank of the rats. Once established, tumors of ~1,500 mm$^3$ were surgically excised and smaller tumor fragments (20-30 mg) were s.c. implanted in the right flank of irradiated rats. Oral administration of KRN951 (0.2 or 1 mg/kg) or vehicle was initiated at the day of randomization (day 0). Tumor volume was measured twice weekly with Vernier calipers, and calculated as (length × width$^2$) × 0.5. Relative tumor volume (RTV) was calculated by the formula: RTV at day $x$ = tumor volume at day $x$ / tumor volume at day 0. Percentage tumor growth inhibition (TGI%) was calculated as described previously (19). Statistical analysis of RTV was done using the unpaired $t$ test.

**DCE-MRI.** Athymic rats (RH-rnu/rnu) were s.c. implanted with fresh Calu-6 tumor fragments. Rats were randomized when the tumors reached a volume of 274 to 287 mm$^3$ (day −1). Once-daily p.o. administration of KRN951 or vehicle was initiated the day after randomization (day 0) and continued for 2 weeks (days 0-13).

MRI experiments were carried out at 1.5 T on a whole body magnet (Magnetom Vision, Siemens, Erlangen, Germany) equipped with a flexible receiver coil (circularly polarized). DCE-MRI acquisitions were done on day −1 (before the start of treatment), day 2, day 13, and day 21. On days 2 and 13, the rats were imaged 4 hours after p.o. administration of KRN951. The rat tail vein was cannulated for contrast agent injection before placing the animals in the magnet. During the experiment, rats were anesthetized by an i.m. injection of a mixture of ketamine (Ketamine500, Centravet, France) and xylazine (Rompun, Centravet, France; 2/1, v/v, 70 and 15 mg/kg, respectively). The anesthetized rats were placed in a cradle supine position inside the resonator. The exact position of the rats was assessed by a scout imaging sequence.

After localization of the tumor in the transverse and sagittal planes using a $T_1$-weighted sequence, a multislice $T_2$-weighted turbo spin-echo sequence was used for acquisition of morphologic images in the transverse plane (repetition delay *TR*, 4,500 ms; echo delay *TE*, 54 ms; image matrix, 126 × 256; field of view *FOV*, 54 × 104 mm; slice thickness, 2 mm). Before DCE-MRI, a calibration procedure took place whereby a $T_1$-weighted gradient echo sequence (FLASH 2D) was used with increasing flip angles from 10° to 90° (repetition delay *TR*, 200 ms; echo delay *TE*, 6 ms; image matrix, 64 × 128; field of view *FOV*, 40 × 80 mm; slice thickness, 3 mm). This process allowed for determination of the correct tumor $T_1$ value before gadolinium-diethylenetriaminepentaacetic acid (Gd-DTPA) injection and was done with a $MnCl_2$ tube of known $T_1$ placed beside the tumor. Subsequently, four precontrast images were acquired with the same technique followed by a rapid bolus i.v. injection of Gd-DTPA at 0.15 mmol/kg. A series of 80 postcontrast images were acquired over 20 minutes with a temporal resolution of 15 seconds per image. Acquisition variables were as follows: repetition delay *TR*, 200 ms; echo delay *TE*, 6 ms; image matrix, 64 × 128; field of view *FOV*, 40 × 80 mm; slice thickness, 3 mm; Flip angle α, 90°.

To determine surrogate markers of capillary permeability and extracellular-extravascular volume using quantitative DCE-MRI, the plasma and tumor Gd-DTPA concentrations were determined as a function of time using the following equation:

$$C(t) = 1/r_1 \times (1/T_1 - 1/T_{10})$$

where $C(t)$ represents the gadolinium concentration as a function of time either in tumor or blood plasma (mmol/L), $r_1$ is the gadolinium relaxivity (mmol/s/L), $T_1$ represents the postcontrast $T_1$ value during bolus passage, and $T_{10}$ represents the precontrast $T_1$ value.

The blood plasma Gd-DTPA concentration was determined by drawing a region of interest (ROI) within the vena cava lumen present in the MR field of view of one or more slices. A postcontrast signal intensity-time curve was obtained and converted into a $T_1$-time curve postinjection. The precontrast $T_1$ value, $T_{10}$, was obtained by converting the precontrast signal intensity averaged over the ROI signal intensities from the four images acquired precontrast. A Gd-DTPA concentration-time curve in blood plasma was calculated using the equation given above. A biexponential fit to the experimental gadolinium concentration-time curve obtained was done using the following equation described by Tofts et al. (23):

$$C(t)_{plasma} = D(a1\exp(-m1t) + a2\exp(-m2t))$$

where $D$ represents the dose of Gd-DTPA in mmol/kg and $a_1$, $a_2$, $m_1$, and $m_2$ $m_2$ are the variables estimated by the fitting procedure and used to describe the blood plasma washout curve of Gd-DTPA.

This procedure has already been described for the quantification of capillary permeability ($K^{trans}$; ref. 23). A permeable membrane separated the compartments of interest; the plasma compartment and the lesion leakage space. The transfer constant linking the two compartments, $K^{trans}$ (per minute), represents the permeability-surface area product per unit volume of tissue ($PS/V_t$). This variable was estimated by applying the following equation to the experimental data:

$$C_T(t) = ve\,Ce(t)$$

where $C_T(t)$ represents the contrast agent concentration within the tumor as a function of time and $Ce(t)$ represents the extravascular-extracellular contrast agent concentration as a function of time.

$K^{trans}$ was estimated over manually drawn ROIs within the periphery and center of the tumor. Enhanced and nonenhanced regions of the tumor were

visually compared, as well as ROIs drawn in the muscle tissue or the kidneys, to confirm the complete perfusion of the contrast agent.

Values were expressed as means ± SD. Statistical analysis was done using the unpaired *t* test.

**Measurement of tumor vessel diameter.** During the MRI study, an additional three groups of Calu-6 tumor-bearing rats (RH-rnu/rnu, three rats per group) were used for measurement of tumor vessel diameter using the fluorescent dye H33342 (24). Rats were treated with KRN951 (0.2 or 1 mg/kg) or vehicle for 14 days (from day 0 to day 13) and were sacrificed 1 minute after the i.v. injection of H33342 (20 mg/kg) at day 13. The tumors were removed and 10 μm cryosections prepared from five levels of each tumor separated by at least 200 μm. Tumor sections were studied under UV illumination using a Nikon epifluorescence microscope (Eclipse 600; Nikon, Tokyo, Japan) to identify blood vessels with a surrounding halo of fluorescent H33342-labeled cells. The lumen enclosed by the halos was measured as the vessel diameter using Win ROOF software (Mitani Corp, Fukui, Japan). Statistical analysis was done using the Mann-Whitney test.

**Histologic analysis of smooth muscle actin–positive pericyte coverage of tumor vessels.** Calu-6 tumor xenografts were established in athymic rats by s.c. implantation of cells. Rats were randomized when tumor volumes reached an average of 273 to 275 $mm^3$ and then treated p.o. with KRN951 or vehicle for 2 weeks. Immunofluorescence staining of pericytes in tumors was done with Cy3-conjugated monoclonal anti-α-smooth muscle actin antibody (Sigma, Saint Louis, MO) following the staining of endothelial cells with anti-CD31 antibody. Tissue images were captured digitally at ×100 magnification with LSM 510 systems (Version 3.2; Carl Zeiss MicroImaging, Inc., Thornwood, NY). Six fields per section (0.8489 $mm^2$ each) were randomly analyzed, excluding peripheral surrounding connective tissues and central necrotic tissues. The number of CD31-positive objects and those surrounded by the region positive for α-smooth muscle actin were quantified using Win ROOF software (Mitani) after blind-coding the histology slides to avoid operator bias.

**Pharmacokinetic analysis of KRN951.** Athymic rats (F344/N JcL-rnu, four females per group) received KRN951 p.o. and blood samples were collected from their tail vein at predetermined intervals up to 72 hours postdose. An appropriate amount of internal standard material, KRN633 (19), was added to each serum sample. Serum samples were deproteinated with acetonitrile and supernatants were analyzed by high-performance liquid chromatography–tandem mass spectrometry. Pharmacokinetic variables were calculated by noncompartmental analysis. The serum concentration of KRN951 at steady state after repeated p.o. administrations of a 0.2 mg/kg dose was simulated as described previously (19).

## Results

**KRN951 activity against receptor tyrosine kinases.** The direct activity of KRN951 against various tyrosine kinases was evaluated using a cell-free kinase assay with recombinant enzymes. KRN951 strongly inhibited VEGFR-1, VEGFR-2, and VEGFR-3 tyrosine kinases ($IC_{50}$ = 30, 6.5, and 15 nmol/L, respectively) and also inhibited EphB2, PDGFR-α, PDGFR-β, c-Kit, and Tie2 tyrosine kinases ($IC_{50}$ = 24, 40, 49, 78, and 78 nmol/L, respectively). The level of KRN951 activity against several other tyrosine kinases revealed a more comprehensive selectivity with $IC_{50}$ values greater than for VEGFR-2 [e.g., $IC_{50}$ = 480 nmol/L for EphB4; 530 nmol/L for FGFR-1; 550 nmol/L for c-Met; 620 nmol/L for Abl; 960 nmol/L for Src; and >1 μmol/L for FGFR-3, FGFR-4, Flt3, EGFR, ErbB2, insulin-R, Fak, ErbB4, insulin-like growth factor (IGF)-1R, and Jak2].

Similarly, KRN951 markedly inhibited the ligand-induced phosphorylation of VEGFR-1, VEGFR-2, and VEGFR-3 in the cellular assay ($IC_{50}$ values 0.16-0.24 nmol/L; Table 1). Although KRN951 also inhibited c-Kit and PDGFR-β phosphorylation, the $IC_{50}$ values were ~10-fold higher than for VEGFR-2. The KRN951 activity level against the phosphorylation of FGFR-1, Flt3, c-Met EGFR, and IGF-IR was considerably lower.

**KRN951 selectively inhibits VEGF signaling responses in endothelial cells.** High concentrations of KRN951 (>0.3 nmol/L) were found to inhibit VEGF-stimulated VEGFR-2 phosphorylation (Fig. 1*B*). Consistent with this, KRN951 strongly inhibited VEGF-dependent phosphorylation of MAPKs in HUVECs (Fig. 1*B*), demonstrating $IC_{50}$ values of 0.13 and 0.18 nmol/L for extracellular signal-regulated kinase 1 (ERK1) and ERK2, respectively. In contrast, KRN951 had little or no effect on bFGF-dependent and EGF-dependent phosphorylation of MAPKs. As shown in Fig. 1*C*, KRN951 inhibited the VEGF-induced proliferation of HUVECs at very low concentrations ($IC_{50}$ = 0.67 nmol/L). Conversely, the inhibitory activity of KRN951 against bFGF-induced proliferation was weak ($IC_{50}$ > 300 nmol/L). Thus, the selectivity of KRN951 for VEGF-induced mitogenic responses, rather than for bFGF- or EGF-induced responses, is consistent with receptor selectivity. In addition, KRN951 at 1 nmol/L reduced the VEGF-mediated migration of HUVECs by ~40% (Fig. 1*D*). At concentrations of

**Table 1.** Effects of KRN951 on the ligand-stimulated phosphorylation of receptor tyrosine kinases

| RTK | Cell | $IC_{50}$ (nmol/L) | 95% Confidence interval (nmol/L) | Fold selectivity vs VEGFR-2* |
|---|---|---|---|---|
| VEGFR-2 | HUVEC | 0.16 | 0.13-0.20 | 1 |
| VEGFR-1 | NIH3T3-Flt-1 † | 0.21 | 0.16-0.30 | 1.3 |
| VEGFR-3 | HUVEC | 0.24 | 0.16-0.34 | 1.5 |
| c-Kit | KU812F | 1.63 | 1.13-2.35 | 10 |
| PDGFR-β | NHDF | 1.72 | 1.39-2.13 | 11 |
| Flt3 | Eol-1 | 422 | 342-522 | 2,640 |
| FGFR1 | NHDF | 299 | 214-417 | 1,870 |
| c-Met | A431 | 1,360 | 730-2,540 | 8,500 |
| EGFR | A431 | ND ‡ | — | — |
| IGF-1R | HT29 | ND ‡ | — | — |

NOTE: $IC_{50}$ values and their 95% confidence intervals were calculated by nonlinear regression analysis of the percentage inhibitions ($n$ = 4).
Abbreviations: NHDF, normal human dermal fibroblast; RTK, receptor tyrosine kinase; ND, not determined.
*Ratio for the $IC_{50}$ was obtained with a given RTK compared with that achieved against VEGFR-2.
†Flt-1–transfected NIH3T3.
‡$IC_{50}$ values could not be determined because KRN951 was apparently insoluble in the medium at the concentrations tested.

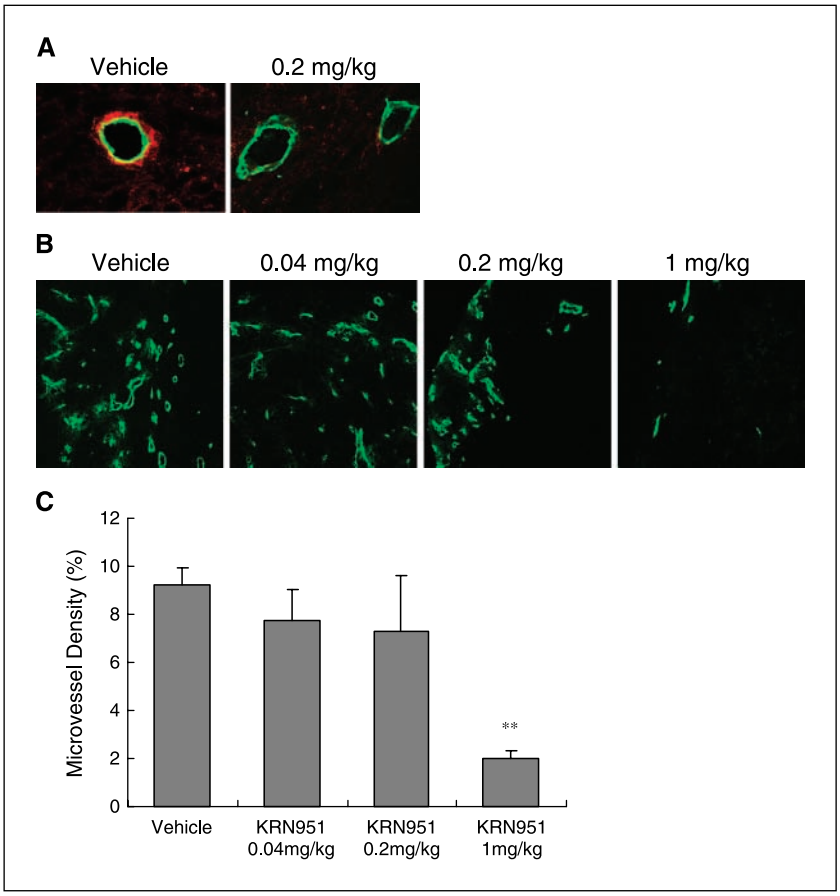


**Figure 2.** Effects of KRN951 on VEGFR-2 phosphorylation levels on tumor endothelium and tumor microvessel density. Athymic rats bearing A549 tumors were treated with KRN951 at the doses indicated, or with vehicle. *A,* tumors were harvested 4 hours after a single oral administration. Cryosections were subjected to immunofluorescence staining for CD31 (*fluorescent green*) and phosphorylated VEGFR-2 (*fluorescent red*) to measure phosphorylation levels of VEGFR-2 on tumor endothelium (magnification ×400). *B,* after 7 days of once-daily treatment with KRN951 or vehicle, cryosections of the tumors were immunostained for CD31 (*fluorescent green*) to quantify microvessel density (magnification ×200). *C,* microvessel density (percentage of CD31-positive area per viable tumor area) was determined by image analysis. *Columns,* means; *bars,* SE. *P* values were calculated with respect to the control (vehicle) group using Dunnett's test. **, $P < 0.01$.

≥10 nmol/L, KRN951 completely inhibited VEGF-induced cell migration.

**KRN951 suppresses phosphorylated VEGFR-2 on tumor endothelium and tumor angiogenesis following p.o. administration.** The A549 tumors from control rats that received vehicle only showed colocalization of fluorescent green staining of CD31 with fluorescent red staining of phosphorylated VEGFR-2. In contrast, tumors from rats that received a single dosing of 0.2 mg/kg KRN951 showed apparent attenuation of VEGFR-2 phosphorylation on the tumor endothelium (Fig. 2*A*). Once-daily p.o. administrations of 0.04, 0.2, or 1.0 mg/kg KRN951 for 7 days resulted in a reduction in the numbers of CD31-positive cells in viable regions of the implanted A549 tumors in athymic rats by 15.7%, 20.7%, and 78.2%, respectively ($P < 0.01$) compared with vehicle treatment alone (Fig. 2*B* and *C*). In addition, H&E staining indicated that KRN951 increased the percentage of necrotic areas within the tumors (data not shown). Tumor growths were almost completely inhibited during the treatment at doses of 0.2 and 1 mg/kg KRN951 (data not shown). These doses resulted in tumor regression of 2% and 33%, respectively.

**Effects of KRN951 on tumor xenograft growth in athymic rats.** The antitumor effects of KRN951 on various human tumors were evaluated in athymic rat xenograft models of breast, colon, hepatic, lung, ovarian, pancreatic, and prostate tumors. The results are summarized in Table 2. After once-daily p.o. administrations of KRN951 for 2 weeks, statistically significant inhibition of tumor growth ($P < 0.05$) was observed in 10 of 14 models receiving a 0.2 mg/kg dose. A significant and almost complete inhibition of tumor growth (TGI > 85%) was observed in 11 of 14 models receiving a 1.0 mg/kg dose. In addition, tumor regression occurred following treatment with KRN951 at 1.0 mg/kg in the MDA-MB-231 and LoVo models (smallest RTV = 0.89 at day 7 and 0.85 at day 21, respectively). Although KRN951 administration did not produce significant antitumor effects in the DU145, CGL-9, or Caki-1 models because of large variations in tumor volumes of vehicle-treated rats, it nevertheless showed a tendency to inhibit the growth of these tumor xenografts in a dose-dependent manner.

KRN951 also induced a loss of rat body weight following the administration of 1.0 mg/kg dosages in some models; however, these weight losses recovered quickly after completion of administration. No body weight losses were observed at 0.2 mg/kg dosages, suggesting that KRN951 is well tolerated at efficacious dosages. No substantial effects following treatment with up to a few μmol/L KRN951 were observed on the *in vitro* growth of cancer cell lines, some of which were used in the xenograft rat models, suggesting that KRN951 is not toxic to cancer cells (data not shown).

**Effects of KRN951 on vascular permeability in Calu-6 tumors: analysis using DCE-MRI.** To evaluate the effects of KRN951 on tumor vascular function and correlate these with its antitumor activities, Calu-6 tumor-bearing rats were subjected to DCE-MRI analysis. The $T_2$-weighted MRI revealed that tumor growth was markedly inhibited in rats treated with 0.2 or 1.0 mg/kg KRN951 between days 6 and 21 and days 2 and 21, respectively, when compared with vehicle-treated rats (Fig. 3*A*). The $K^{trans}$ values in the rim of the tumor were significantly decreased (by 45%) at day 13 in rats treated with 0.2 mg/kg KRN951, and at day 2 (by 55%) and day 13 (by 61%) in rats treated with 1 mg/kg KRN951, when compared with vehicle-treated rats (Fig. 3*B*). These

**Table 2.** Effects of KRN951 on human tumor xenografts in athymic rats

| Cell | Tumor type | Initial tumor volume ($mm^3$) | TGI% | |
|---|---|---|---|---|
| | | | 0.2 mg/kg | 1.0 mg/kg |
| MDA-MB-231 | Breast | 495 | 77.0* | >100* |
| ZR-75-1 | Breast | 522 | 77.2* | 94.3* |
| LoVo | Colon | 658 | 60.3* | >100* |
| LS174T | Colon | 785 | 85.7* | 99.7* |
| SK-HEP-1 | Liver | 404 | 59.4* | 89.9* |
| Calu-6 | Lung | 592 | 44.1* | 99.2* |
| NCI-H460 | Lung | 765 | 68.8* | 85.9* |
| OVCAR-3 | Ovarian | 504 | 25.0 | 98.5* |
| SK-OV-3 | Ovarian | 625 | 93.4* | 99.2* |
| BxPC-3 | Pancreas | 510 | 60.7* | 93.5* |
| DU145 | Prostate | 535 | 90.6 | >100 |
| PC-3 | Prostate | 376 | 73.6* | 95.9* |
| CGL-9 | Glioma | 325 | 46.0 | 96.2 |
| Caki-1 | Renal | 444 | 26.9 | >100 |

NOTE: The percentage of tumor-growth inhibition (TGI%) compared with the vehicle-treated group was calculated on the day after the last treatment (day 14) except for the TGI% for BxPC-3, which was calculated on day 13.
*$P < 0.05$.

effects were more pronounced in the Calu-6 tumor rim than in the tumor center (data not shown). No significant difference in $K^{trans}$ was observed after day 21 for KRN951-treated rats compared with vehicle-treated rats, suggesting that the effects on vascular permeability in those tumors were reversible after drug withdrawal.

**Effects of KRN951 on vessel diameter and pericyte coverage.** The tumor vessels in Calu-6 tumor-bearing rats were identified in all histologic sections by the surrounding halo of fluorescent H33342-labeled cells. As shown in Fig. 4, the median lumen area enclosed by the halos in tumors of rats treated with 0.2 and 1 mg/kg KRN951 was significantly larger (57.9 and 65.8 μm, respectively; Fig. 4*B*) than in tumors of vehicle-treated rats on day 13 (43.2 μm). The ratio of enlarged vessels with a diameter of >100 μm increased in tumors from rats treated with 0.2 and 1 mg/kg KRN951 (24.3% and 30.3%, respectively) when compared with rats treated with vehicle (17.5%). In addition, tumor sections from KRN951-treated rats exhibited a greater staining intensity than those from vehicle-treated rats. Pericyte coverage of tumor vessels was further analyzed by dual immunostaining with anti-CD31 antibody and anti–α-smooth muscle actin-antibody, which detect endothelial cells and pericytes, respectively. After 14 days of therapy, the proportion of endothelial cells associated with pericytes increased from 20.7% in the vehicle-treated group to 29.6% in the 0.2 mg/kg KRN951 group and 50.5% in the 1 mg/kg KNR951 group ($P < 0.01$; Fig. 4*C*). Simultaneously, treatment with 0.2 and 1 mg/kg KRN951 decreased microvessel density by 42.5% ($P < 0.01$) and 71.2% ($P < 0.001$) compared with vehicle, respectively (data not shown).

**Pharmacokinetic profile of p.o. administered KRN951 in athymic rats.** Rat KRN951 serum concentration after p.o. administration was determined to confirm exposure, and pharmacokinetic analysis was done to analyze the correlation with its efficacy (Supplementary Table S1). The area under the serum concentration-time curve from zero to infinity ($AUC_{inf}$) was 0.34, 1.64, 7.64, and 44.5 μg·h/mL and the $C_{max}$ was 21.6, 108, 484, and 2,823 ng/mL after a single p.o. administration of 0.04, 0.2, 1, or 5 mg/kg KRN951, respectively. In the 0.04 to 5 mg/kg range, both the $AUC_{inf}$ and $C_{max}$ of KRN951 increased in proportion to the dose, whereas p.o. clearance (CL/*f*), apparent distribution volume ($V_d/F$), and elimination half-life ($t_{1/2}$) were similar, suggesting that KRN951 has an approximately linear pharmacokinetic profile in female athymic rats in this dose range. Pharmacokinetic simulation analysis was also carried out in which KRN951 achieved steady state soon after repeated p.o. administration (data not shown). The trough concentration at steady-state ($C_{min}^{ss}$), the maximum concentration at steady-state ($C_{max}^{ss}$), and the average concentration at steady-state ($C_{av}^{ss}$) of 0.2 mg/kg/d KRN951 were simulated to be 22.2, 124, and 69.5 ng/mL, respectively (data not shown).

## Discussion

It is now widely accepted that VEGF signaling through the VEGFR-2 in endothelial cells is primarily responsible for tumor

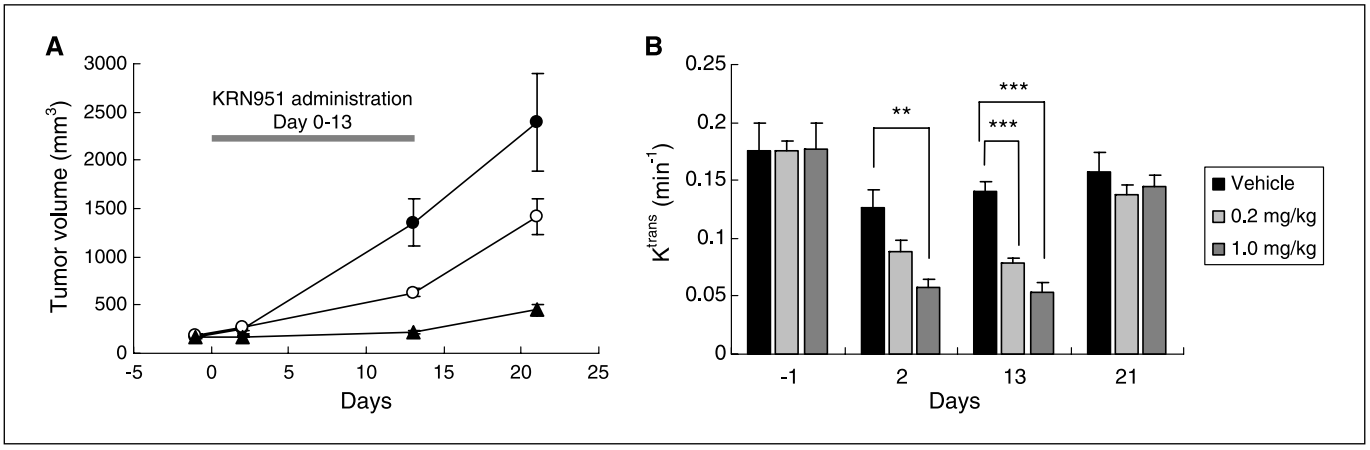


**Figure 3.** DCE-MRI analysis of tumor vascular permeability. Athymic rats bearing Calu-6 tumors were randomized at day −1 and then treated with 0.2 mg/kg KRN951 (○), 1 mg/kg KRN951 (▲), or vehicle (●) once daily for 14 days (days 0-13). At the days indicated, contrast agent (Gd-DTPA) was injected i.v. before MRI analysis. $T_2$-weighted anatomic and $T_1$-weighted perfusion images were taken to indicate localization and contrast agent uptake of tumors, respectively. *A,* tumor volumes were determined by MRI analysis. *B,* capillary permeability ($K^{trans}$) in tumors was calculated from perfusion curves, which were generated from ROIs on the periphery of the tumor. *P* values were calculated by comparing with the vehicle-treated group using the unpaired *t* test. **, $P < 0.01$; ***, $P < 0.001$.

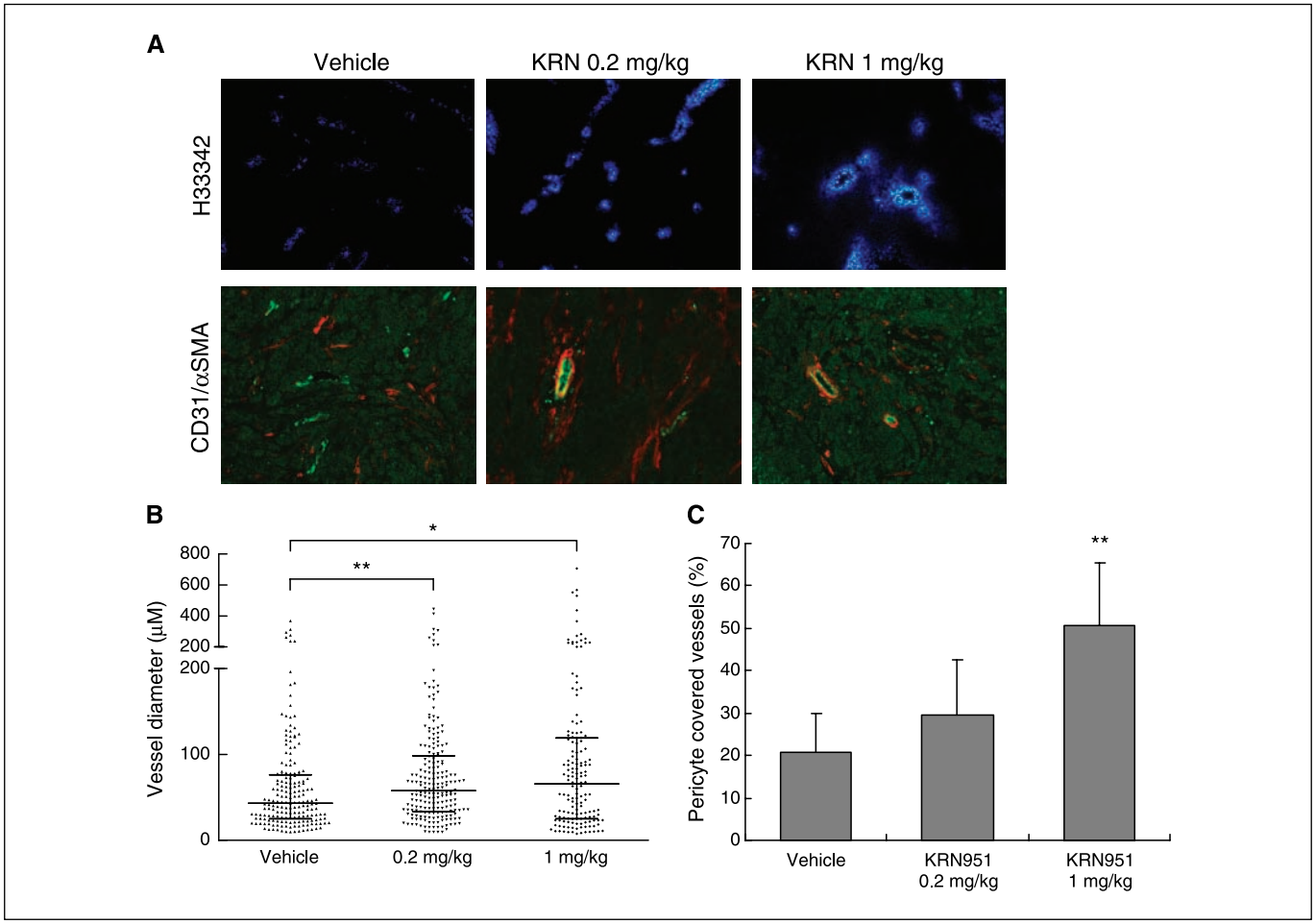


**Figure 4.** Effects of KRN951 on tumor vessel diameter and pericyte coverage. Tumor-bearing rats were treated with vehicle or KRN951 for 14 days. Cryosections of the tumor tissues were prepared following i.v. injection of H33342 fluorescent dye for assessment of vessel diameter ($n = 3$). Paraffin sections were also prepared for assessment of pericyte coverage of tumor vessels ($n = 6$). *A,* representative images of tumor sections from rats treated with vehicle, 0.2 mg/kg KRN951, and 1 mg/kg KRN951 were captured under UV illumination (*top*) or using a fluorescent microscope (*bottom*) at ×200 magnification for assessment of vessel diameter or pericyte coverage of tumor vessels, respectively. *Blue,* H33342; *green,* CD31-positive endothelial cells; *red*, α-smooth muscle actin-positive pericytes. *B,* the length of the major axis of the halos related to H33342 (*blue fluorescence*) was determined by imaging analysis. A column scatter plot shows each value in a group. The superimposed line represents the median and interquartile range of the group. *P* values were calculated with respect to the control (vehicle) group using the Mann-Whitney test. *, $P < 0.05$; **, $P < 0.01$. *C,* the percentage of pericyte coverage on tumor-associated endothelial cells was determined by counting positive vessels in six fields within each individual tumor and six tumors per group as described Materials and Methods. *P* values were calculated with respect to the control group using Dunnett's test. **, $P < 0.01$.

angiogenesis. In this study, we showed the direct activity of KRN951 against VEGFR-2 tyrosine kinase using recombinant proteins, which led to the inhibition of VEGF-stimulated VEGFR-2 phosphorylation in endothelial cells. The selectivity of KRN951 for VEGFR-2 tyrosine kinase was confirmed in both cell-free and cell-based assays. These results are consistent with the ability of KRN951 to inhibit VEGF-driven, but not bFGF- or EGF-driven, phosphorylation of MAPK and cell proliferation. In addition, we showed that VEGF-mediated cell migration, which precedes cell proliferation and is essential for angiogenesis, was inhibited by KRN951. We also showed that p.o. administration of KRN951 significantly reduced microvessel density in tumors and inhibited tumor growth across multiple organ-specific tumor types in rat xenograft models, despite the absence of cytotoxic effects during *in vitro* cell growth. In a similar *in vivo* model, we observed a decrease in VEGFR-2 phosphorylation on tumor endothelium after KRN951 treatment, indicating that the primary *in vivo* target of KRN951 is VEGFR-2 phosphorylation. On the other hand, the angiogenic program triggered by VEGFs may involve possible heterodimerization between VEGFR-1, VEGFR-2, and VEGFR-3. The effects of KRN951 on these heterodimer complexes remains to be shown. However, this may not be an important consideration as it seems that the major angiogenic signals elicited by VEGF are mediated by the VEGFR-2 homodimer complex (1). In addition, KRN951 would be expected to act on heterodimer complexes as well, based on its property as a pan-VEGFR tyrosine kinase inhibitor. Accordingly, it is clear that KRN951 is a highly potent VEGFR-2 tyrosine kinase inhibitor with antitumor and antiangiogenesis properties that might be applicable for the treatment of solid tumors and other diseases involving pathologic angiogenesis.

Although many synthetic VEGFR-2 tyrosine kinase inhibitors have been reported (13–21), it is worth noting that KRN951 possesses significantly more potent *in vitro* and *in vivo* activities in comparison. KRN951 inhibited VEGF-dependent proliferation of HUVECs with an $IC_{50}$ of 0.67 nmol/L, whereas in similar assays, PTK787/ZK 222584 (13), SU11248 (14), CP-547,632 (15), and

KRN633 (19, 20) showed higher $IC_{50}$ values of 7.1, 4, 14, and 15 nmol/L, respectively. Only AZD2171 (21) shows a comparable level of inhibition ($IC_{50}$ = 0.4 nmol/L).

The strong *in vivo* activities of KRN951 probably reflect its high activity *in vitro*. Indeed, we observed severely reduced levels of phosphorylated VEGFR-2 on tumor endothelial cells and significant and broad-spectrum antitumor activities at very low doses (0.2 or 1 mg/kg/d) following single and repeated administration, respectively. In view of this and considering the results of clinical investigations into angiogenesis inhibitors, such as PTK787 (25), pharmacologically active KRN951 serum concentrations are expected to be easily achievable. Moreover, it is likely that KRN951 would produce broader antitumor activities as a pan-VEGFR inhibitor than other compounds, such as specific antibodies targeting the VEGF and VEGFR-2 systems. KRN951 shows almost equipotent *in vitro* anti-VEGFR-1 and anti-VEGFR-3 tyrosine kinase activities, and it is expected that the extent of *in vivo* inhibition would be similar. Recent studies have suggested that signaling through VEGFR-1 is directly or indirectly involved in tumor angiogenesis in several types of cancer (26–30). In addition, it has been reported that signaling through VEGFR-3 plays an important role in lymphangiogenesis and may be involved in lymphatic metastasis (31, 32).

Enzyme and receptor phosphorylation data have shown that KRN951 is selective in its VEGFR tyrosine kinase activity, a feature that distinguishes it from other dual-targeted or multitargeted small-molecule inhibitors, such as AZD2171 (targeting both VEGFR and c-Kit), SU11248 (targeting VEGFR, PDGFR, c-Kit, and Flt3), or BAY 43-9006 (targeting VEGFR, PDGFR, c-Kit, Flt3, and Raf-1). Although the inhibition of cancer-associated kinases by these multitargeted agents could provide additional therapeutic benefit in the treatment of certain types of tumors, it could lead to unwanted adverse side effects in patients through the inhibition of the physiologic function of the target kinase. For example, c-Kit plays an important role in the growth of gastrointestinal stromal tumors (33) and acute myeloid leukemia (34), but it is also critical in the development of the interstitial cells of Cajal, which show pacemaker activity (35, 36). It is therefore possible that c-Kit inhibition would cause gastrointestinal malfunctions such as diarrhea. Thus, selective VEGFR inhibitors are welcome from a safety viewpoint, particularly in cases where the tumors are less likely to depend on alternative kinases.

Progress in molecular-targeted cancer therapeutics highlights the need for suitable biomarkers to evaluate the efficacy of such treatments. Until recently, the most widely used method to analyze angiogenesis inhibitors was the qualification of intratumoral microvessel density in tumor biopsies. As a repeatable, noninvasive technique, DCE-MRI has been successfully used to assess the response to various antiangiogenic treatments, including VEGFR inhibitors in preclinical and clinical settings (37–39). The current study therefore used DCE-MRI to examine the antitumor and antiangiogenic activities of KRN951 in a preclinical model. A significant change in tumor vascular permeability was successfully detected after only 3 days of treatment, suggesting that DCE-MRI analysis is well adapted for the early detection of tumor response to KRN951 treatment and that $K^{trans}$ could be a suitable noninvasive biomarker of KRN951 activity in a clinical setting.

Interestingly, treatment with KRN951 not only reduced microvessel density, but also enlarged the diameter of the remaining functional vessels in the tumors. A similar phenomenon has been reported following treatment with other VEGFR inhibitors (37). In addition, tumor sections from KRN951-treated rats exhibited a greater staining intensity around the vessels than those of vehicle-treated rats, leading us to speculate that tumor interstitial pressure is decreased after KRN951 treatment. An attractive hypothesis recently advanced by Jain (40) proposes that some antiangiogenic agents could inhibit both new tumor vessel formation (neoangiogenesis) and transiently "normalize" the abnormal structure and function of tumor vasculature to enhance oxygen permeation and drug delivery. The "vascular normalization" hypothesis predicts that a VEGFR-2 blockade would result in an increase in pericyte coverage of tumor vessels (41). Indeed, KRN951 increased the proportion of endothelial cells associated with pericytes, favoring this hypothesis. Of course, it could be assumed that this increase is still due to the preferential pruning of pericyte-poor vessels (42, 43). However, if the vascular normalization theory were validated, antiangiogenic therapy could be administered together with cytotoxic drugs, rendering it more effective in combating tumors. Whatever the exact mechanism of action of such a combined therapy, a recent study with bevacizumab provides definitive proof of the efficacy of angiogenesis inhibitors when combined with a chemotherapeutic regimen in the clinic (44). The enlargement of tumor vessel diameter and the increase in pericyte coverage after KRN951 treatment can be explained by this theory, suggesting a possible mode of action for KRN951 when associated with another anticancer agent.

It is conceivable that the knowledge of the target serum concentration, particularly of molecular-targeted drugs, would enable the design of appropriate regimens to ensure constant target suppression and the selection of individual dose optimizations in a clinical setting. The pharmacokinetic and pharmacodynamics analysis in the current study revealed that simulated KRN951 concentrations of ~70 ng/mL (~140 nmol/L) are sufficient to inhibit tumor growth in rats after oral administration. This estimate is much higher than the *in vitro* concentrations required to inhibit VEGF signaling and is likely due to plasma protein binding of KRN951, because our preliminary data indicate that the plasma protein binding ratio is >99% in rats. Follow-up studies are being conducted to define the pharmacokinetic variables that drive efficacy.

In this article, we describe the characterization of KRN951, a p.o. bioavailable angiogenesis inhibitor targeting VEGFR tyrosine kinases with potent antitumor efficacy. We also show that DCE-MRI is useful in detecting the *in vivo* antiangiogenic efficacy of KRN951 at an early stage of treatment. Furthermore, we show pharmacokinetic profiles that estimate the KRN951 serum concentration necessary for its *in vivo* antitumor efficacy. These results provide a basic rationale for further investigation of KRN951 as an antitumor agent in clinical settings. KRN951 is currently under evaluation in a phase I clinical trial.

## Acknowledgments

Received 12/1/2005; revised 6/27/2006; accepted 7/11/2006.

The costs of publication of this article were defrayed in part by the payment of page charges. This article must therefore be hereby marked *advertisement* in accordance with 18 U.S.C. Section 1734 solely to indicate this fact.

We thank Teruyuki Sakai for helpful comments, and Yoshiko Tazunoki, Ikuko Nagahune, Yoshiko Kobayashi, Noriko Takahashi, and Hideko Murooka for their excellent technical assistance.

## References


1. Ferrara N, Gerber HP, LeCouter J. The biology of VEGF and its receptors. Nat Med 2003;9:669–76.
2. Harris AL. Hypoxia—a key regulatory factor in tumour growth. Nat Rev Cancer 2002;2:38–47.
3. Weidner N. Intratumor microvessel density as a prognostic factor in cancer. Am J Pathol 1995;147:9–19.
4. Dvorak HF. Vascular permeability factor/vascular endothelial growth factor: a critical cytokine in tumor angiogenesis and a potential target for diagnosis and therapy. J Clin Oncol 2002;20:4368–80.
5. Toi M, Matsumoto T, Bando H. Vascular endothelial growth factor: its prognostic, predictive, and therapeutic implications. Lancet Oncol 2001;2:667–73.
6. Hasan J, Byers R, Jayson GC. Intra-tumoural microvessel density in human solid tumours. Br J Cancer 2002; 86:1566–77.
7. List AF. Vascular endothelial growth factor signaling pathway as an emerging target in hematologic malignancies. Oncologist 2001;6 Suppl 5:24–31.
8. Veikkola T, Karkkainen M, Claesson-Welsh L, Alitalo K. Regulation of angiogenesis via vascular endothelial growth factor receptors. Cancer Res 2000;60:203–12.
9. Shibuya M. Structure and function of VEGF/VEGF-receptor system involved in angiogenesis. Cell Struct Funct 2001;26:25–35.
10. Glade-Bender J, Kandel JJ, Yamashiro DJ. VEGF blocking therapy in the treatment of cancer. Expert Opin Biol Ther 2003;3:263–76.
11. Herbst RS, Onn A, Sandler A. Angiogenesis and lung cancer: prognostic and therapeutic implications. J Clin Oncol 2005;23:3243–56.
12. Ferrara N, Hillan KJ, Gerber HP, Novotny W. Discovery and development of bevacizumab, an anti-VEGF antibody for treating cancer. Nat Rev Drug Discov 2004;3:391–400.
13. Wood JM, Bold G, Buchdunger E, et al. PTK787/ZK 222584, a novel and potent inhibitor of vascular endothelial growth factor receptor tyrosine kinases, impairs vascular endothelial growth factor-induced responses and tumor growth after oral administration. Cancer Res 2000;60:2178–89.
14. Mendel DB, Laird AD, Xin X, et al. *In vivo* antitumor activity of SU11248, a novel tyrosine kinase inhibitor targeting vascular endothelial growth factor and platelet-derived growth factor receptors: determination of a pharmacokinetic/pharmacodynamic relationship. Clin Cancer Res 2003;9:327–37.
15. Ruggeri B, Singh J, Gingrich D, et al. CEP-7055: a novel, orally active pan inhibitor of vascular endothelial growth factor receptor tyrosine kinases with potent antiangiogenic activity and antitumor efficacy in preclinical models. Cancer Res 2003;63:5978–91.
16. Beebe JS, Jani JP, Knauth E, et al. Pharmacological characterization of CP-547,632, a novel vascular endothelial growth factor receptor-2 tyrosine kinase inhibitor for cancer therapy. Cancer Res 2003;63:7301–9.
17. Wilhelm SM, Carter C, Tang L, et al. BAY 43-9006 exhibits broad spectrum oral antitumor activity and targets the RAF/MEK/ERK pathway and receptor tyrosine kinases involved in tumor progression and angiogenesis. Cancer Res 2004;64:7099–109.
18. Sepp-Lorenzino L, Rands E, Mao X, et al. A novel orally bioavailable inhibitor of kinase insert domain-containing receptor induces antiangiogenic effects and prevents tumor growth *in vivo*. Cancer Res 2004;64: 751–6.
19. Nakamura K, Yamamoto A, Kamishohara M, et al. KRN633: A selective inhibitor of vascular endothelial growth factor receptor-2 tyrosine kinase that suppresses tumor angiogenesis and growth. Mol Cancer Ther 2004; 3:1639–49.
20. Matsunaga N, Nakamura K, Yamamoto A, Taguchi E, Tsunoda H, Takahashi K. Improvement by solid dispersion of the bioavailability of KRN633, a selective inhibitor of VEGF receptor-2 tyrosine kinase, and identification of its potential therapeutic window. Mol Cancer Ther 2006;5:80–8.
21. Wedge SR, Kendrew J, Hennequin LF, et al. AZD2171: a highly potent, orally bioavailable, vascular endothelial growth factor receptor-2 tyrosine kinase inhibitor for the treatment of cancer. Cancer Res 2005;65:4389–400.
22. Sawano A, Takahashi T, Yamaguchi S, Aonuma M, Shibuya M. Flt-1 but not KDR/Flk-1 tyrosine kinase is a receptor for placenta growth factor, which is related to vascular endothelial growth factor. Cell Growth Differ 1996;7:213–21.
23. Tofts PS, Kermode AG. Measurement of the blood-brain barrier permeability and leakage space using dynamic MR imaging. 1. Fundamental concepts. Magn Reson Med 1991;17:357–67.
24. Ljungkvist AS, Bussink J, Rijken PF, Kaanders JH, van der Kogel AJ, Denekamp J. Vascular architecture, hypoxia, and proliferation in first-generation xenografts of human head-and-neck squamous cell carcinomas. Int J Radiat Oncol Biol Phys 2002;54:215–28.
25. Mross K, Drevs J, Muller M, et al. Phase I clinical and pharmacokinetic study of PTK/ZK, a multiple VEGF receptor inhibitor, in patients with liver metastases from solid tumours. Eur J Cancer 2005;41:1291–9.
26. Salven P, Lymboussaki A, Heikkila P, et al. Vascular endothelial growth factors VEGF-B and VEGF-C are expressed in human tumors. Am J Pathol 1998;153: 103–8.
27. Donnini S, Machein MR, Plate KH, Weich HA. Expression and localization of placenta growth factor and PlGF receptors in human meningiomas. J Pathol 1999;189:66–71.
28. Hiratsuka S, Maru Y, Okada A, Seiki M, Noda T, Shibuya M. Involvement of Flt-1 tyrosine kinase (vascular endothelial growth factor receptor-1) in pathological angiogenesis. Cancer Res 2001;61:1207–13.
29. Autiero M, Waltenberger J, Communi D, et al. Role of PlGF in the intra- and intermolecular cross talk between the VEGF receptors Flt1 and Flk1. Nat Med 2003;9:936–43.
30. Luttun A, Autiero M, Tjwa M, Carmeliet P. Genetic dissection of tumor angiogenesis: are PlGF and VEGFR-1 novel anti-cancer targets? Biochim Biophys Acta 2004; 1654:79–94.
31. Alitalo K, Carmeliet P. Molecular mechanisms of lymphangiogenesis in health and disease. Cancer Cell 2002;1:219–27.
32. He Y, Karpanen T, Alitalo K. Role of lymphangiogenic factors in tumor metastasis. Biochim Biophys Acta 2004; 1654:3–12.
33. Rubin BP, Singer S, Tsao C, et al. KIT activation is a ubiquitous feature of gastrointestinal stromal tumors. Cancer Res 2001;61:8118–21.
34. Beghini A, Ripamonti CB, Cairoli R, et al. KIT activating mutations: incidence in adult and pediatric acute myeloid leukemia, and identification of an internal tandem duplication. Haematologica 2004;89: 920–5.
35. Maeda H, Yamagata A, Nishikawa S, et al. Requirement of c-kit for development of intestinal pacemaker system. Development 1992;116:369–75.
36. Huizinga JD, Thuneberg L, Kluppel M, Malysz J, Mikkelsen HB, Bernstein A. W/kit gene required for interstitial cells of Cajal and for intestinal pacemaker activity. Nature 1995;373:347–9.
37. Drevs J, Muller-Driver R, Wittig C, et al. PTK787/ZK 222584, a specific vascular endothelial growth factor-receptor tyrosine kinase inhibitor, affects the anatomy of the tumor vascular bed and the functional vascular properties as detected by dynamic enhanced magnetic resonance imaging. Cancer Res 2002;62:4015–22.
38. Morgan B, Thomas AL, Drevs J, et al. Dynamic contrast-enhanced magnetic resonance imaging as a biomarker for the pharmacological response of PTK787/ZK 222584, an inhibitor of the vascular endothelial growth factor receptor tyrosine kinases, in patients with advanced colorectal cancer and liver metastases: results from two phase I studies. J Clin Oncol 2003;21:3955–64.
39. Miller JC, Pien HH, Sahani D, Sorensen AG, Thrall JH. Imaging angiogenesis: applications and potential for drug development. J Natl Cancer Inst 2005;97:172–87.
40. Jain RK. Normalization of tumor vasculature: an emerging concept in antiangiogenic therapy. Science 2005;307:58–62.
41. Winkler F, Kozin SV, Tong RT, et al. Kinetics of vascular normalization by VEGFR2 blockade governs brain tumor response to radiation: role of oxygenation, angiopoietin-1, and matrix metalloproteinases. Cancer Cell 2004;6:553–63.
42. Benjamin LE, Golijanin D, Itin A, Pode D, Keshet E. Selective ablation of immature blood vessels in established human tumors follows vascular endothelial growth factor withdrawal. J Clin Invest 1999;103:159–65.
43. Gee MS, Procopio WN, Makonnen S, Feldman MD, Yeilding NM, Lee WM. Tumor vessel development and maturation impose limits on the effectiveness of anti-vascular therapy. Am J Pathol 2003;162:183–93.
44. Hurwitz H, Fehrenbacher L, Novotny W, et al. Bevacizumab plus irinotecan, fluorouracil, and leucovorin for metastatic colorectal cancer. N Engl J Med 2004;350:2335–42.